Towards a System for Modeling the Impact of Ocean Acidification on Sea Scallops (*Placopecten magellanicus*) in Massachusetts Bay

Patrick Wahlig

Under the direction of

Dr. Pierre F. J. Lermusiaux
Professor of Mechanical Engineering and Ocean Science and Engineering
Massachusetts Institute of Technology

Dr. Patrick J. Haley
Research Scientist
Massachusetts Institute of Technology

Research Science Institute
December 11, 2022

Abstract

The world's oceans serve a critical role in absorbing CO_2 emissions, but this process contributes to rising ocean acidity. Northern coastal bodies of water like Massachusetts Bay are especially susceptible to ocean acidification. Massachusetts Bay supports a strong mollusk fishery, including the economically important Atlantic sea scallop (*Placopecten magellanicus*). As oceans acidify, the saturation state of aragonite, a mineral critical in mollusk shell formation, decreases, impeding shellfish development. In this study, a program was designed to evaluate the impact of ocean acidification on sea scallop growth in Massachusetts Bay. Equations modeling shellfish growth from previous literature were analyzed, and relevant formulae extracted and compiled. The resultant program was coupled to an existing MIT-MSEAS PE model. Initial parameters were sourced from recent population assessments. A total of four experimental scenarios were run for 32.5 days, each scenario depicting a varying dependency on three variables: aragonite availability, temperature, and physical phenomena (e.g., tides, winds, solitons, density-driven flow, internal waves). Growth of Massachusetts Bay sea scallops was found to depend heavily on aragonite saturation. Examined in isolation, variations in initial temperature did not substantially affect sea scallop growth. The incorporation of physical phenomena, however, resulted in subtle changes in scallop growth, demonstrating that ocean dynamics play an important role in temperature redistribution. Similarly, when both aragonite concentration and physical phenomena were incorporated into the model, the resultant effect on scallop growth indicated that ocean dynamics are a crucial driver of aragonite distribution as well. Coupling a shellfish growth submodel to the MIT-MSEAS PE allowed successful modeling of the impact of aragonite, temperature, and physical phenomena on sea scallop growth in Massachusetts Bay.

Summary

Levels of atmospheric carbon dioxide have increased as a result of human activity, causing oceans to acidify. Northern coastal waters like Massachusetts Bay are especially vulnerable to ocean acidification. As oceans acidify, the volume of minerals used in mollusk shell formation (e.g., aragonite) decreases. This study designed a computer program modeling the impact of ocean acidification on shellfish growth in Massachusetts Bay. Due to their vital economic importance, sea scallops were selected as the study species. Four scenarios were run, each with different variable dependencies. The results show that sea scallops rely heavily on aragonite saturation to grow and develop. The effects of temperature appear less significant and nearly uniform across locations. Physical dynamics are found to be critical in transporting aragonite to deepwater environments and considerably impact the growth of sea scallops.

1 Introduction

Worldwide, levels of atmospheric carbon dioxide (CO_2) continue to rise dramatically. Anthropogenic CO_2 emissions are of special concern, as they have exhibited an exponential pattern of growth since measurements were first taken at the Mauna Loa Observatory in 1958 [1]. Recent estimates by Friedlingstein et al. [2] place total anthropogenic CO_2 emissions from 1850 to 2020 at close to 2420 gigatons of CO_2. Elevated levels of atmospheric CO_2 trap more radiation, warming the earth and damaging the biosphere [3, 4]. If unaddressed, these emissions can precipitate natural disasters, scarcity of natural resources, and political discord [5].

Acting as carbon sinks, the world's oceans are critical in countering elevated levels of CO_2 in the atmosphere. Since the beginning of the industrial era, oceans have absorbed almost half (48%) of all anthropogenic CO_2 emissions [6]. This buffer process releases hydrogen protons (H^+), decreasing ocean pH levels and increasing ocean acidity [7]. Not all marine zones are equally affected by ocean acidification. Coastal waters are particularly vulnerable, as elevated rates of freshwater input negatively impact buffering capability [8]. Northern waters exhibit lower buffering capacity than their southern counterparts due to lower average temperatures. Combining both of these features, northern New England coastal waters (e.g., Massachusetts Bay) are therefore especially imperiled by ocean acidification [9].

As oceanic pH levels decrease, the availability of calcium carbonate polymorphs like aragonite and calcite (minerals critical for shellfish growth and development) also decreases [10]. Of special concern is the decrease in aragonite saturation (Ω) due to ocean acidification. Aragonite is a more soluble form of calcium carbonate than calcite and is relied upon by shellfish larvae for initial shell formation [11]. The heightened solubility of aragonite, however, makes it susceptible to ocean acidification, which corrodes aragonite [12]. A decrease in the saturation state of aragonite negatively impacts shellfish growth, initiating a decline

in shellfish population size [12]. Ecologically, shellfish serve as critical building blocks of the complex oceanic trophic system. Acting as "ecosystem engineers", shellfish filter water, combat erosion, and create habitable environments for other species [13]. Due to the durability of mollusk shells, this role persists long after shellfish death [14]. Shellfish contribute significantly to the global economy, but projections show that ocean acidification may lead to a $100 billion loss in shellfish-generated revenue by the year 2100 [15].

Of particular relevance to the Atlantic coast is the Atlantic sea scallop (*Placopecten magellanicus*). This species is of regional economic importance, with the 2019 commercial sea scallop harvest generating over $570 million in landings [16]. Although primarily concentrated on Georges Bank and the Mid-Atlantic Bight, sea scallops are distributed as far south as North Carolina and as far north as Newfoundland [17]. In the acidification-prone waters of Massachusetts Bay, a population exists along Stellwagen Bank [18]. In order to protect this ecologically and economically critical species, the impact of ocean acidification on sea scallops must be examined.

This study is designed to demonstrate the relationship between ocean acidification and sea scallop population distribution. Values for ocean acidification variables are first generated by a primitive equation model, then transferred to a scallop growth model. In this study, initial ocean acidification variables (aragonite saturation and temperature) are sourced from a numerical simulation of Massachusetts Bay using the Massachusetts Institute of Technology Multidisciplinary Simulation, Estimation, and Assimilation Systems primitive equation (MIT-MSEAS PE) model. To design an applicable shellfish growth model, existing models were reviewed and the roles of ocean acidification variables in shellfish growth and development were determined. Several shellfish models have been produced previously, but with varied emphasis (e.g., individual growth, scope for growth, population dynamics, fisheries management) [19, 20, 21]. After extensive evaluation, an existing scallop growth model outlined by Cooley et al. [21] in 2015 was selected and adapted to Massachusetts Bay conditions.

In this way, a set of representative equations reflecting shellfish growth was established and coupled to the existing MIT-MSEAS PE model. The resultant program serves as a comprehensive, real-time detection system displaying the impact of ocean acidification on sea scallops in Massachusetts Bay.

2 Methods

2.1 Categorizing Existing Shellfish Growth Models

First current progress in shellfish growth modeling was reviewed. Available models had a wide range of applications, forcing variables, and conclusions [22, 23]. The pool of models was divided into two categories for further analysis: individual growth models and population dynamics models. Individual growth models were found to often rely on dynamic energy budget (DEB) theory. DEB theory is a metabolic theory that represents organism energy use, reproduction, and development as functions of size and environmental interactions [24]. In addition, DEB theory is general and easily applied to a wide range of species across developmental stages [25]. Models implementing DEB theory, however, did not reflect the influence of established ocean acidification variables [26]. In contrast, population dynamics models incorporated a larger bank of equations for a detailed analysis of an entire population. Within these equations, especially those related to scallop growth and recruitment, variables influenced by ocean acidification were found to play primary roles [21].

2.2 Suitability of Model Categories for Project Goals

This study determined that the ideal method of measuring the impact of ocean acidification on Atlantic coast shellfish would utilize population dynamics models. Individual growth models, although more simple, would reveal less information on the overall state of a

species as compared to population dynamics models. Several models integrating temperature [23, 27] were identified. Only one (Cooley et al., 2015) [21] addressed a second relevant ocean acidification variable: aragonite. Following the process outlined by Cooley et al., the current study adapts and couples this model to the MIT-MSEAS PE model and is the first to apply it to sea scallops in the Massachusetts Bay area.

2.3 Shellfish Growth & Population Dynamics Equations

The shellfish submodel nested in the integrated assessment model designed by Cooley et al. was selected as most suitable for modeling sea scallop response to ocean acidification [21]. Unless otherwise stated, all equations below are sourced from the integrated assessment model outlined in the Cooley study.

According to the shellfish submodel, total scallop population size is comprised of several size class bins, which scale by 5 mm intervals. Scallops enter the first bin at the shell height H of 40 mm, which corresponds to the time that they recruit into the general sea scallop population [28]. This study defines the last size bin as having a lower limit of 90 mm and an upper limit of ∞ to account for all sea scallops. The 90mm lower limit corresponds to the 3.5-inch minimum shell height regulation for commercially harvested sea scallops in Massachusetts, leaving open the future possibility of considering fisheries pressures upon this final bin [29].

The number of individuals in each bin comprise h elements that then make up the vector $\vec{n}(t)$. The sum of all the elements of $\vec{n}(t)$ represents the total sea sea scallop population at each time step t (yr).

The total count of scallops in each size class is given as:

$$\vec{n}(t + \Delta t) = \vec{R}\Delta t + \boldsymbol{G_t} \cdot \ e^{-(M)\Delta t} \cdot \ \vec{n}(t) \tag{1}$$

where $\vec{n}(t+\Delta t)$ is the vector representing the subsequent scallop population (millions) after the time step is applied, $\vec{R}$ is a measure of recruitment (individuals yr^{-1}), Δt is the change in time (yr), $\boldsymbol{G_t}$ is a matrix which denotes the probability of advancing bins, M is a measure of natural mortality (yr^{-1}), and $\vec{n}(t)$ signifies the scallop population before the time step is applied.

The equation modeling recruitment is defined as:

$$\vec{R} = \frac{\alpha_R SSB}{\gamma_R + SSB} \tag{2}$$

where α_R is defined as the recruitment asymptote (millions of individuals), γ_R is defined as the half saturation coefficient (mT meats), and SSB is the spawning stock biomass (mT meats). The values for α_R and γ_R were obtained from the Georges Bank initial parameters outlined in Cooley, et al. [21]. Scallops only recruit into the first $(40-45$ mm) size class. For simplicity, this study assumes that the recruitment rate is constant throughout the year.

To model the impact of aragonite saturation state ($\Omega_{aragonite}$) on scallop recruitment, an empirical scale factor is computed to be applied to initial spawning stock biomass ($SSBi$):

$$SSB\ scale\ factor = \frac{\%\ survival}{\%\ average\ survival} = \frac{(20.5\Omega_{aragonite}\ -\ 3.7)}{45} \tag{3}$$

where $\%\ survival$ is represented by the function $(20.5\Omega_{aragonite}\ -\ 3.7)$. The value for $\%\ average\ survival$ is given as 45 in accordance with control survival rates of great scallops (*Pecten maximus*) established by Andersen et al. [30]. This scale factor is then applied to $SSBi$ following the relationship outlined in Equation 4:

$$scaled\ SSB = (SSB_i)\ (SSB\ scale\ factor) \tag{4}$$

where *scaled SSB* is the output to be used in quantifying R, $SSBi$ is initial spawning stock biomass, and $SSB\ scale\ factor$ is the scale factor applied to initial spawning stock biomass. Calculated at each hour-long advance in time, *scaled SSB* serves as an input to Equation 2, which models sea scallop recruitment adjusted for aragonite saturation.

The growth matrix $\boldsymbol{G_t}$ describes scallop growth across size classes at every active grid point. In general, $\boldsymbol{G_t}$ is a square matrix of size $(n_{\text{bins}} \cdot n_{\text{gridpoints}}) \times (n_{\text{bins}} \cdot n_{\text{gridpoints}})$ where n_{bins} is the total number of size classes being considered and $n_{\text{gridpoints}}$ is the number of active grid points (points where scallops are being modeled). This study's program contained 13,139 active locations. $\boldsymbol{G_t}$ becomes especially tractable when the following modeling assumptions are made.

1. Scallop growth at one grid point is not affected by scallop growth at any other grid point. This encompasses both the notion that scallops do not move frequently enough to travel between grid points and the idea that scallop growth does not impact the physical fields (temperature, aragonite) that are controlling growth. Under this assumption, $\boldsymbol{G_t}$ becomes block diagonal with $n_{\text{gridpoints}}$ block sub-matrices, $\hat{\boldsymbol{G}}_{\boldsymbol{t}}$, of size $n_{\text{bins}} \times n_{\text{bins}}$.

2. The time step Δt is small enough that scallops cannot "jump" size classes (e.g., scallops from size class $i-1$ can grow into size class i but scallops from size classes $1, 2, \therefore, i-2$ cannot). With this assumption each of the block sub-matrices, $\hat{\boldsymbol{G}}_{\boldsymbol{t}}$, becomes bi-diagonal with the nonzero elements restricted to the main diagonal and to the first sub-diagonal.

If the probability of a scallop growing out of size class i is denoted as P_i, then each of the elements, $\hat{G}_{t;(i,j)}$, of $\hat{\boldsymbol{G}}_{\boldsymbol{t}}$ can be written as:

$$\hat{G}_{t;(i,j)} = \begin{cases} 1 - P_i & j = i; \quad i \in \{1, 2, \ldots, n_{\text{bins}}\} \\ P_{i-1} & j = (i-1); \quad i \in \{2, 3, \ldots, n_{\text{bins}}\} \\ 0 & \text{otherwise} \end{cases} \tag{5}$$

To evaluate P_i, the range of shall lengths that could grow out of size class i is estimated by computing how much growth a shell beginning as the upper limit of size class i can grow in time Δt (ΔH). Then, it is assumed that any scallop of shell length within ΔH of the upper limit will grow out of size class i. Finally, it is assumed that the scallop shell lengths within a size class are uniformly distributed in that size class, so the probability is ratio of the lengths:

$$P_i = \frac{H_{t+\Delta t} - H_t}{Bin\ Width} = \frac{\Delta H}{Bin\ Width} \tag{6}$$

where $H_{t+\Delta t}$ is shell length (mm) after the change in time, H_t signifies shell length before the time step is applied, and $Bin\ Width$ represents the width of the size bin (5 mm).

Change in shell length ΔH is represented by:

$$\Delta H = (H_\infty - H_t)\ (1 - e^{-K\Delta t}) \tag{7}$$

where H_∞ is asymptotic length (mm) and K is the Brody growth coefficient, a measure of how fast it takes for an organism to reach maximum length.

K is calibrated to both temperature and aragonite. To calculate change in K because of change in aragonite saturation, it is first necessary to determine the relative change in aragonite from the control:

$$\Delta\Omega = \frac{\Omega}{\Omega_{control}} - 1 \tag{8}$$

where $\Delta\Omega$ is the relative change in aragonite from the control, Ω is the measured aragonite saturation state, and $\Omega_{control}$ is the control aragonite saturation state.

Then, change in growth rate is represented by the empirical equation:

$$\Delta G = 1.272\Delta\Omega + 0.075 \tag{9}$$

where ΔG is a measure of relative change in growth rate.

Finally, assuming that the relative change in G is equal to the relative change in K, change in K from the initial value is generated by multiplying relative change in growth rate by the Brody growth coefficient:

$$\Delta K_\Omega = \Delta G \cdot K_i \tag{10}$$

where ΔK_Ω is the relative change in K from the initial value K_i due to change in aragonite saturation.

To calibrate K to change in temperature, this study drew from empirical temperature-growth relationships outlined in Heilmayer et al. [31] and determined that the sum of K_i and the change in K due to temperature can be represented by the empirical equation:

$$K_i + \Delta K_T = \frac{e^{e^{4.22-958.466\cdot\frac{1}{T}}}}{M_\infty} \tag{11}$$

where $K + \Delta K_T$ represents K plus the change in K due to temperature, T is a measure of temperature (kelvin), and M_∞ is the asymptotic total weight (g).

After the outputs of Equations 10 and 11 are calculated, overall change in K due to change in T and Ω can be summed:

$$K_{T,\Omega} = K_i + \Delta K_T + \Delta K_\Omega \tag{12}$$

where $K_{T,\Omega}$ represents change in K due to both temperature and aragonite saturation.

2.4 Identification of Suitable Input Parameters

Several parameters from Cooley et al. [21] were adjusted. Population size (millions), length frequencies, and $SSBi$ (mT meats) were determined according to data collected by Lisi et al. in 2021 [18]. Asymptotic total weight M_∞ was calculated following total weight to meat weight relationships outlined by Hennen and Hart [32]. A value for the control saturation state of aragonite ($\Omega_{control}$) was obtained by averaging the initial values for Ω at the bottom level around Stellwagen Bank. This study did not consider pressures exerted by fisheries (denoted as Z_t in Cooley et al. [21]), allowing focused examination of the effect of ocean acidification on sea scallop performance. Initial values for dissolved inorganic carbon and total alkalinity were obtained from the MIT-MSEAS PE model and used to compute the aragonite saturation state using the CO2SYS equilibrium [33]. To best reproduce the environmental conditions of Massachusetts Bay, total dissolved inorganic silicon and total dissolved inorganic phosphorus were set at 0 μmol/kg. Standard atmospheric pressure was set at 10.132501 decibars. The K_1 and K_2 dissociation constants were set at 3 in accordance with the conclusions of Hannson refit by Dickson & Millero [34, 35]. The value for the KSO_4 dissociation constant was also set at 3 following the conclusions of Dickson in 1990 [36].

Table 1: Input Parameters for Sea Scallop Growth Model

Parameter	**Value**	**Units**	**Source**	**Use**
$\Omega_{control}$	1.75		MIT-MSEAS PE	Equation 8
$average\ survival$	45	%	[30]	Equation 3
K_i	0.429	yr^{-1}	[21]	Equation 10
M_∞	467.685	grams	[21, 32]	Equation 11
$SSBi$	1013	mT meats	[18]	Equation 4
α_R	20.17	millions	[21, 37, 38]	Equation 2
γ_R	6.664	mT meats	[21, 37, 38]	Equation 2
H_∞	144.9	millimeters	[21, 37]	Equation 7
M	0.12	yr^{-1}	[21, 37]	Equation 1

2.5 Program Design

The scallop growth program's code was written in MATLAB, following a modular and flexible design approach. The program was designed from the top-down and written from the bottom-up. Construction began with the first equations necessary to calculate the variables involved in Equation 1 (e.g., Equation 3, Equation 8). Each function was unit tested along the build process. Substituting simple values for variables ensured that each individual file was performing as intended and that any subsequent errors would not be related to coding errors in functions already passing the unit tests. Values of aragonite saturation and temperature were passed to the functions through one-way coupling (without feedback) to the MIT-MSEAS PE model. The computational domain for the Massachusetts Bay simulation is shown in Figure 1.

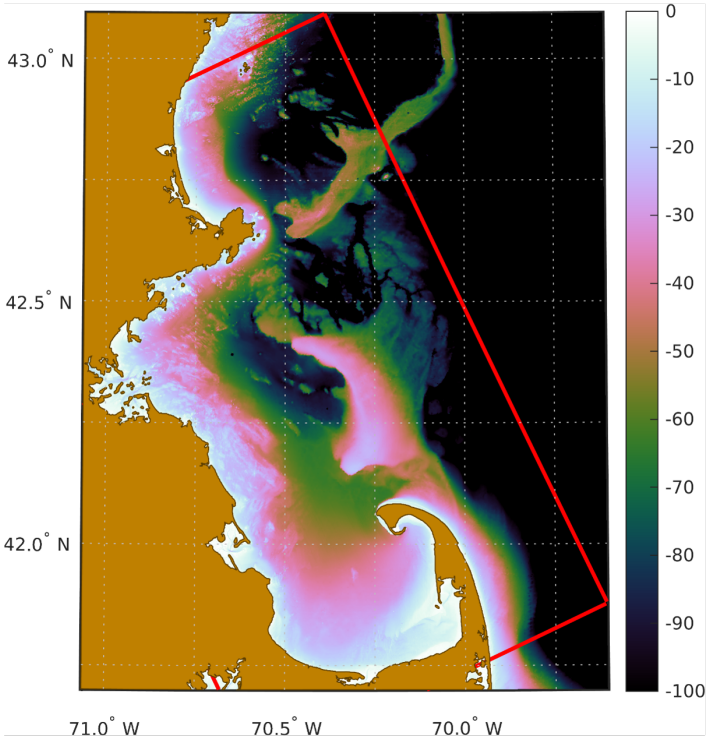

Figure 1: Bathymetry chart of Massachusetts Bay providing visual representation of depth (meters) by location [39]. The modeling domain of the MIT-MSEAS PE model is enclosed by the red border.

2.6 Experimental Scenarios

Based on the initial parameters and equations outlined above, four experimental scenarios were run. The first scenario (Run 1) modeled scallop growth as a function of aragonite saturation, temperature, and physical phenomena (tides, winds, solitons, density-driven flow, internal waves). The second scenario (Run 2) modeled scallop growth as a function of temperature and physical phenomena, but not aragonite saturation. The third scenario (Run 3) modeled scallop growth as a function of temperature only, excluding both aragonite saturation and physical phenomena. The fourth and final scenario (Run 4) modeled scallop growth as a function of aragonite and temperature, but excluded physical phenomena. Each scenario was run from the time period August 11, 2019 to September 13, 2019 to ensure that accurate data from the MIT-MSEAS PE model was utilized.

2.7 Initialization

This study aimed to create initial conditions as representative of the Massachusetts Bay sea scallop population as possible. Although the shallow waters of the Bay hold mainly bay scallops, a sizeable population of sea scallops exists around Stellwagen Bank. Following the conclusions of the 2021 Stellwagen Bank sea scallop population assessment conducted by Lisi et al. [18], a set of area-specific initial conditions (population size, boundary parameters, and length distribution) were developed.

Stellwagen Bank sea scallops were divided into a northern and southern sector. The northern population box had latitudinal boundaries of 42.33° N to 42.62° N and longitudinal boundaries of 70.25° W to 70.67° W. The southern population box had latitudinal boundaries of 42.12° N to 42.33° N and longitudinal boundaries of 70.09° W to 70.44° W. Initial population sizes (89.65 million for the northern box and 17.76 million for the southern box) were assigned evenly within each box. Initial distribution of scallops across the 11 size bins

was calculated using size distribution data from Lisi et al. [18] for each box.

3 Results & Discussion

Within Massachusetts Bay, there exist several dynamical phenomena driving distribution of aragonite and temperature. Internal tides, winds, solitary waves, and background advection of water from the Gulf of Maine all play critical roles in influencing aragonite saturation state and temperature levels [39]. Deep waters such as those on the western border of Northern Stellwagen Bank (Figure 1, 42.3° N 70.5° W) tend to have lower saturation levels of aragonite than shallow waters (Figure 2a). This finding is due to acidic deep-water input from the Gulf of Maine [40], but local tidal and wave patterns result in mixing of aragonite across depths. While aragonite depth distribution without physics appears smoothly stratified (Figure 2a), oceanic disturbances from internal waves, etc. transport highly-saturated surface aragonite down to deeper waters (Figure 2b).

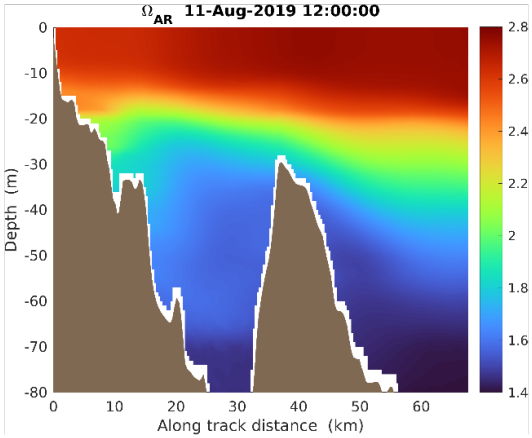

(a) Initial aragonite distribution.

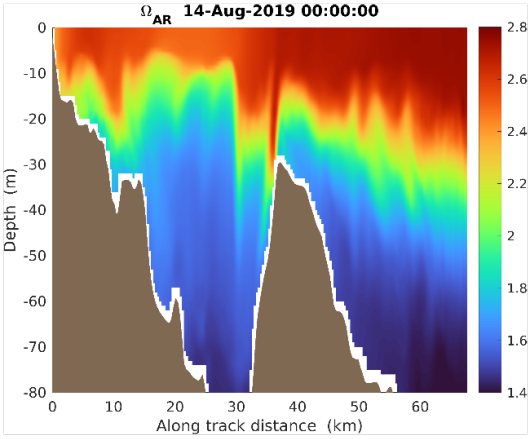

(b) Aragonite distribution after 2.5 days.

Figure 2: Effects of physical phenomena on aragonite distribution by depth over a 2.5-day period [39]. Note the disruption of aragonite stratification in Figure 2b due to the passing of an internal wave. These physical actions bring highly-saturated aragonite to deeper waters, making it more available for use by shellfish.

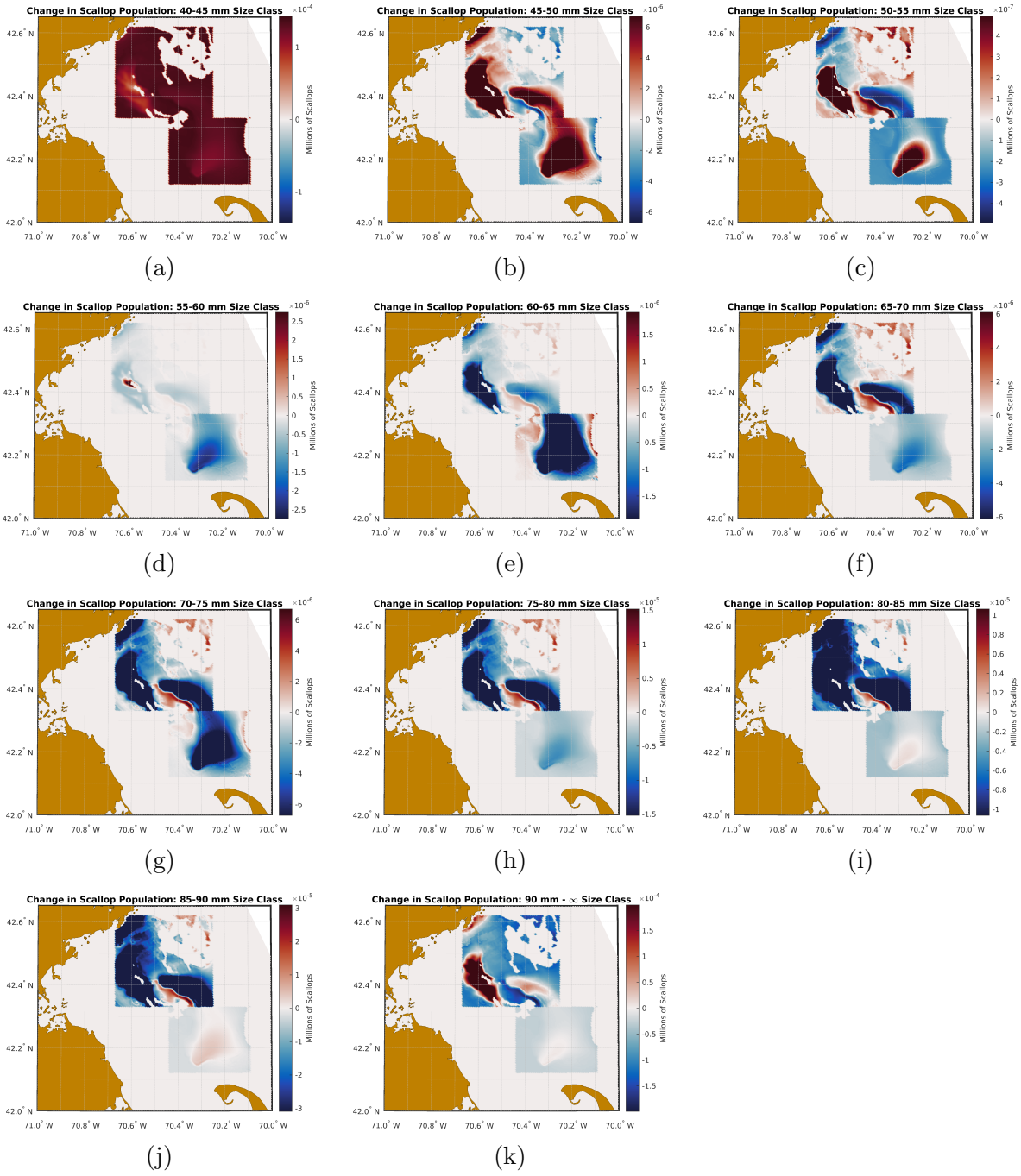

Figure 3: Run 1, change in sea scallop size distribution considering the effects of temperature, aragonite, and physics. Sea scallop growth shows a strong dependency on aragonite and physics. Figure generated by researcher.

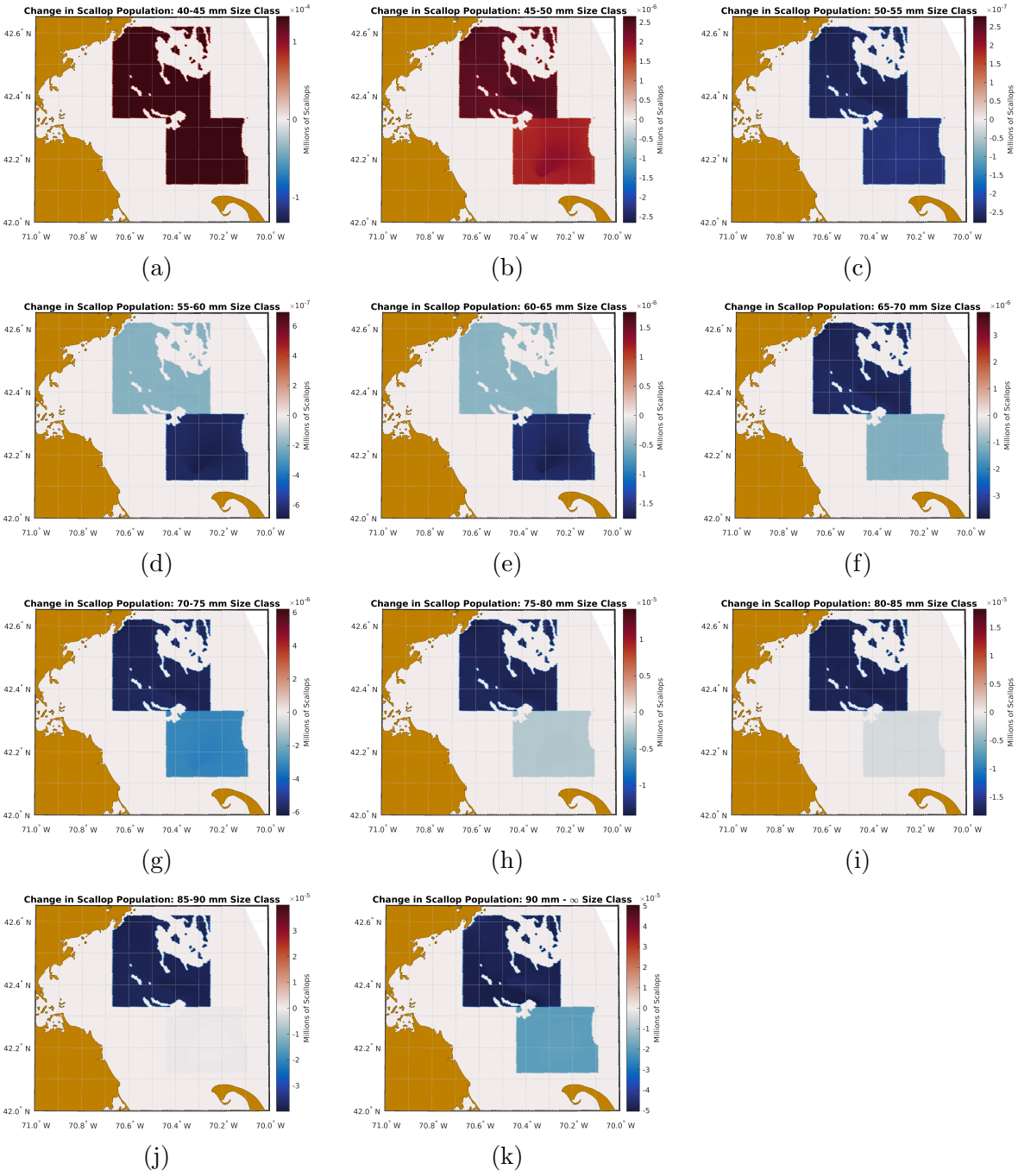

Figure 4: Run 2, change in sea scallop size distribution considering the effects of temperature and physics, but not aragonite. Temperature influence appears fairly uniform, but subtle physical effects are present. Figure generated by researcher.

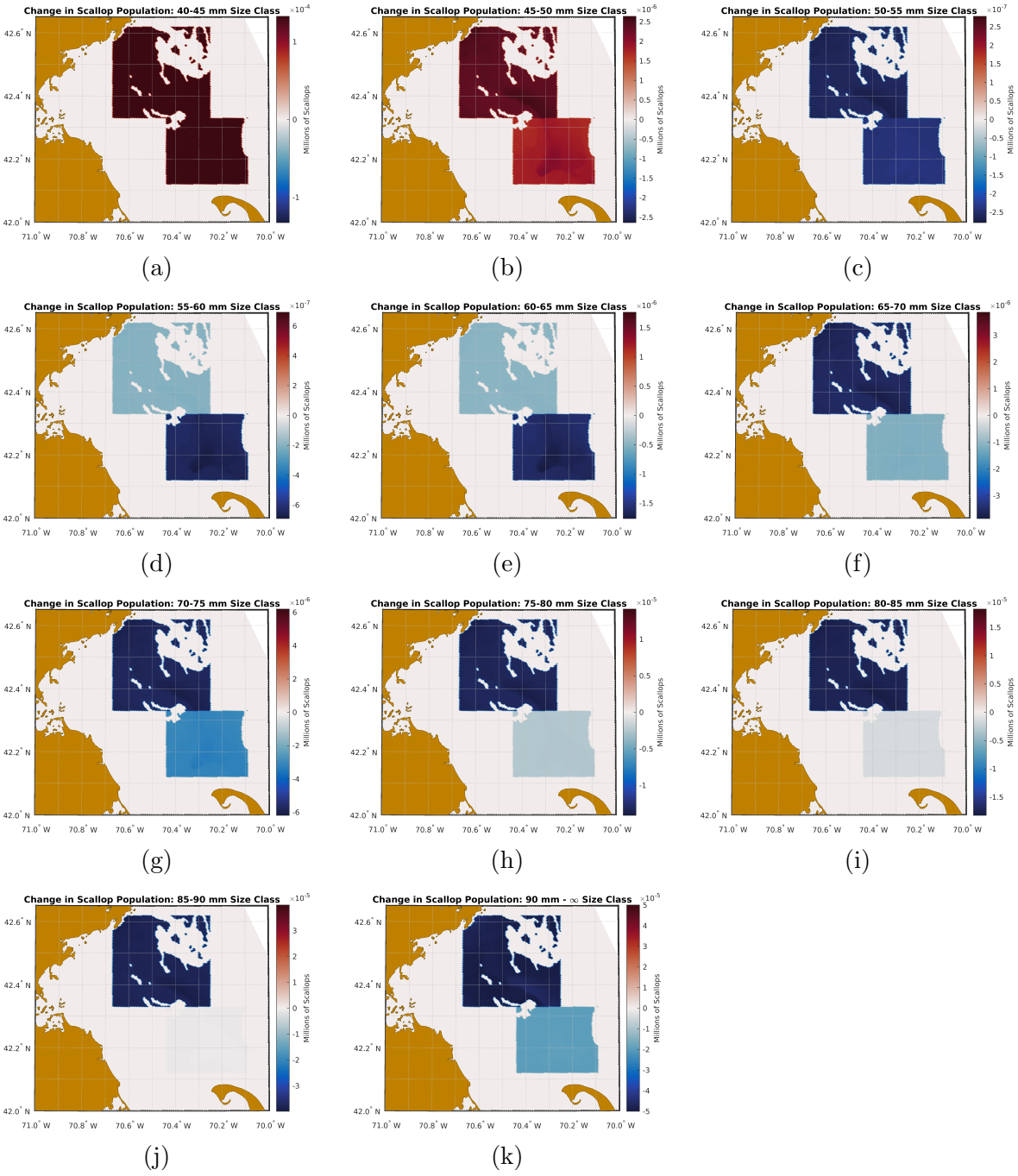

Figure 5: Run 3, change in sea scallop size distribution considering the effects of temperature, but not aragonite or physics. Note that the difference between Run 3 and Run 2 is small, displaying a slight influence of physics on temperature distribution and scallop growth. Figure generated by researcher.

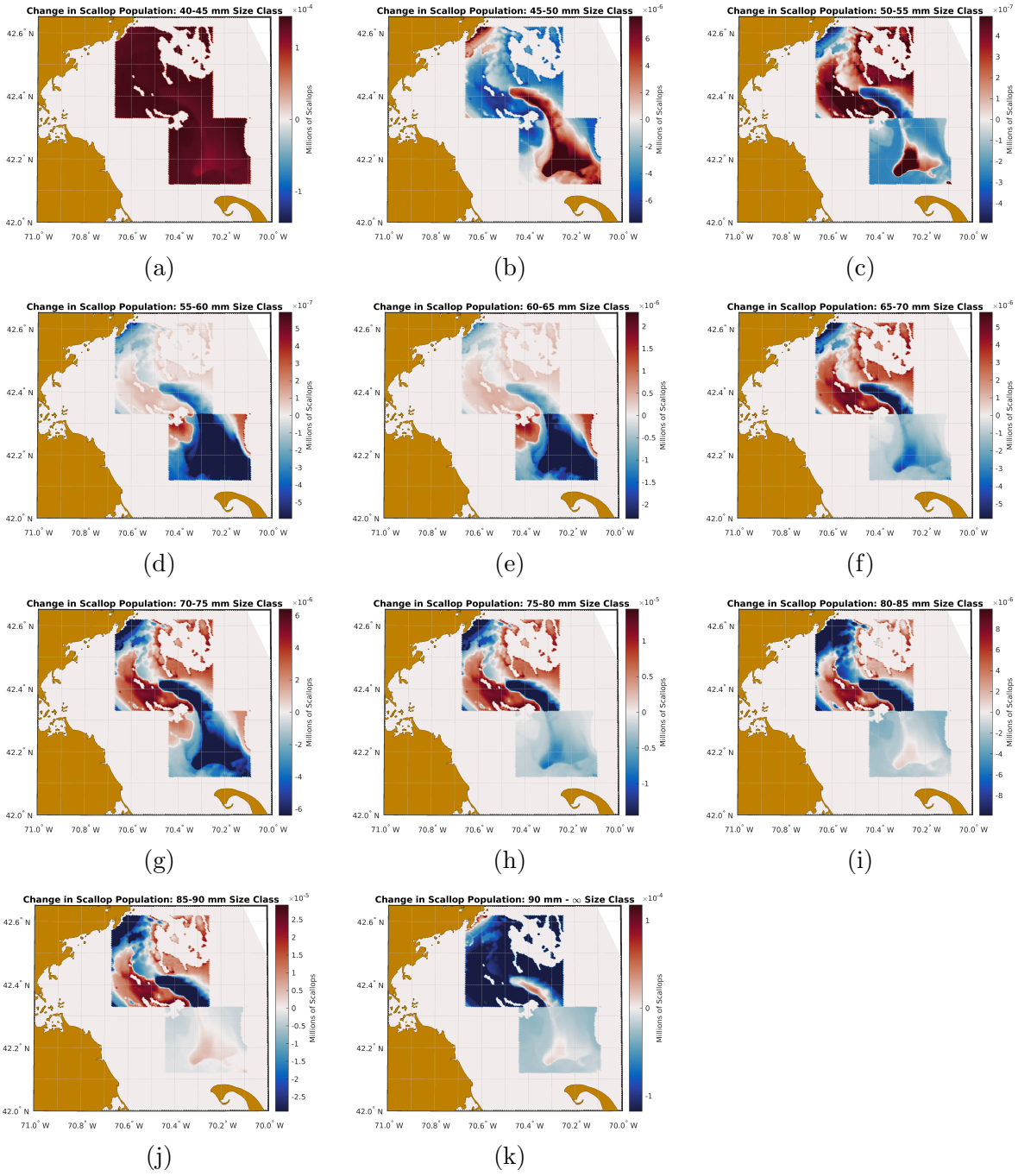

Figure 6: Run 4, change in sea scallop size distribution considering the effects of aragonite and temperature, but not physics. The striking difference between Run 4 and Run 1 highlights the critical role ocean physics plays in aragonite distribution and scallop growth. Figure generated by researcher.

Over the 32.5-day period, the run with full dependency on aragonite, temperature, and physics (Run 1) saw substantial recruitment into the first ($40-45$ mm) size class (Figure 3a). The next two size classes ($45-50$ mm and $50-55$ mm) exhibited increases in population size along the northern box depth decline, and the $50-55$ mm size class saw growth along the western ledge of Northern Stellwagen Bank (Figure 3b, Figure 3c). The $55-60$ mm size class appeared to have sizeable input from the lower size classes within an area of deep water on the western border of Northern Stellwagen Bank (Figure 3d). The southern zone, however, saw net loss in scallop population size. Mortality (M) is constant in the model. Therefore, an abnormal loss in population of a size class can either represent growth out of that size class into the class above, or that the number of scallops exiting the lower size class is less than the combined effect of growth into the upper size class and M. The following 6 size classes ($60-90$ mm) had similar patterns of growth (Figures 3e-3j). While population size increased along the eastern ledge of Northern Stellwagen Bank and in the northeastern corner of the northern box, nearly all other sectors saw a net loss in population size. The final size class (90 mm$-\infty$) exhibited growth along the coastline in the northwest corner of the northern box, the shallow zone of Northern Stellwagen Bank, and the deep zone bordering Northern Stellwagen Bank to the west. Additionally, the southern box exhibited a slight rise in population size within the shallowest area of Southern Stellwagen Bank, though surrounding change was mostly negative (Figure 3k). As dynamical phenomena (e.g., tidal movements, wind, storms) were considered in this run, aragonite saturation varied by location with time. Tidal movements increase mixing of waters, bringing highly saturated aragonite down to deeper waters and promoting growth [39]. This downwelling effect was likely a critical driver of the increased growth within the deep area west of Northern Stellwagen Bank. Overall, full dependency on physics, aragonite, and temperature resulted in remarkable variation in growth within and among size classes.

Run 2, executed with a dependency on temperature and physics, exhibited results similar

to those of Run 3, where temperature was considered but aragonite dependency and physics were excluded. Slight differences were detected among plots, especially in Figures 4b and 5b (size class $45-50$ mm) and Figures 4e and 5e (size class $60-65$ mm). All other plots contained no visible variation. The lack of strong variation between runs displays that the influence of dynamical phenomena on temperature distribution in Massachusetts Bay has little impact on shellfish growth. However, there was a subtle effect of physics on population growth due to temperature over the 32.5-day period. Without physics, more change in population size was identified in shallower/warmer regions. When physics was considered and waters mixed, shallow water-specific growth became less notable. If the simulations were carried out over a longer span of time, this effect would be magnified.

Run 4 considered both temperature and aragonite saturation, but physical phenomena were excluded. Values for temperature and aragonite were read only from the initial conditions. As there was no opportunity for dynamical phenomena to influence the distribution of aragonite or temperature, the results of Run 4 shared little similarity with the results of Run 1. Run 4 saw considerable growth within areas of deeper water surrounding Northern Stellwagen Bank in size classes 6b-6j, but this growth was less frequent in the Run 1. Additionally, the last size class of the fourth run (Figure 6k) exhibited growth on the shallowest areas of Stellwagen Bank, whereas the last size class of Run 1 saw negative growth within these areas (Figure 3k). Dissimilarity between the two runs highlights the vital role that ocean dynamics play on aragonite and temperature distribution, as well as on shellfish growth and development.

4 Future Work

The 32.5-day run period of each experimental scenario provided valuable insight into the role physical phenomena and ocean acidification variables (aragonite saturation, tempera-

ture) play in influencing sea scallop growth. A longer run duration, perhaps over an entire season of growth, may reveal more significant trends. For instance, if the run time of Run 2 was extended, the effect of physical phenomena on temperature distribution may impact a wider range of size classes. An even longer time frame, utilizing data from before the industrial revolution, would convey the impact of anthropogenic ocean acidification over a more sweeping, historical timeframe. Runs observing these long time scales would prove critical in shaping an understanding of how shellfish growth rates are affected by long-term changes in ocean environments. The results generated by this model might also be compared to empirical data to test accuracy. Moreover, forecasting programs could be probabilistic, providing reliability estimates of produced forecasts. Additionally, initial conditions and recruitment parameters could be set as position-dependent, rather than evenly distributed, which would provide a precise profile of ideal growth zones. Such a system would provide invaluable advice to shellfish farms and fisheries management organizations regarding the threat of ocean acidification on a particular shellfish population.

Currently, the model only addresses the impacts of aragonite and temperature on larval survival (equation 2). Unlike their mature counterparts, sea scallop larvae are not fixed to the ocean floor. Instead, they are dispersed throughout the water column [41]. Larvae also have the ability to move and be advected horizontally. Modeled recruitment would be enhanced by functions and/or simulations representing the impact of aragonite and temperature on larvae across a wide depth and area range, rather than limiting these variables to deep-water values.

In Massachusetts Bay, several additional shellfish species exist. Of special relevance is the American oyster, which has substantial ecological and economic value [42]. Due to disease and improper management, American oyster populations have fallen significantly [43]. In fact, estimates conclude that harvest levels of the widely-studied Chesapeake Bay American oyster population have fallen to only 1% of maximal productivity [44, 45, 46]. The equations

and parameters implemented in the current sea scallop model could be adapted to this species, and a growth model could be developed to accurately predict the impact of ocean acidification on the strained American oyster population. Such an adaptation would involve evaluating the implications of shallow-water environments on the MIT-MSEAS PE model and considering the impacts of river input and erosion on coastal environments.

This study did not consider the effects of fishing pressure on modeled sea scallop populations, which assisted in reaching a baseline understanding of the impacts that aragonite, temperature, and dynamical phenomena have on sea scallops. To practically implement such a model into fisheries management, however, fishing mortality and selectivity for certain size classes should be incorporated.

5 Conclusion

When coupled to the MIT-MSEAS PE model, the shellfish growth model successfully projected the impact of aragonite, temperature, and physical phenomena on sea scallop growth in Massachusetts Bay. Trends exhibited in Run 1 displayed a distinct reliance upon aragonite by Massachusetts Bay sea scallops. Due to the wide range in growth rates within and among size classes, it can be concluded that Massachusetts Bay aragonite saturation was not evenly distributed. Temperature effects on sea scallop growth were less obvious (Run 2, Run 3) and appeared relatively uniform in distribution. When physical phenomena were incorporated, the model yielded subtle changes in shellfish growth. A temperature redistribution effect was noted when Run 2 was compared to Run 3. Similarly and more convincingly, when Run 1 and Run 4 are compared, the impact of ocean dynamics on aragonite distribution and scallop growth is demonstrated. Tides, internal waves, wind, and solitons are crucial drivers of this phenomenon, intermittently bringing highly-saturated surface aragonite down to deeper waters inhabited by sea scallops and promoting substantial growth and development. The

shellfish model produced by this study could be enhanced with longer run times and the consideration of fisheries mortality. Longer run times would model the centuries-long impact of ocean acidification on sea scallops, and the consideration of fisheries mortality would facilitate more relevant use by fisheries management organizations.

6 Practical Takeaways

This study's findings have practical applications in the fields of aquaculture, fisheries management, and environmental assessment. The shellfish aquaculture industry is prominent along the Atlantic coast and in the state of Massachusetts, yielding 45.5 million dollars in a 2015 study from Augusto and Holmes [47]. This industry will require consistent growth to meet demand. As oceans acidify and shellfish growth rates slow, it will become harder to sustain the shellfish industry. With slight modification of initial parameters, the model in this study could be implemented by shellfish farmers along the coast. Farmers would be able to determine ideal locations and seasons for growth, increasing efficiency and providing the industry with more resilience against a changing climate.

While aquaculture has the ability to control early stages of growth in shellfish, the Atlantic coast mollusk fishery does not have this advantage. Ocean acidification poses an extreme risk to wild shellfish populations, and must be factored into stock assessments and regulation. The model produced by this study would provide valuable information regarding threatened areas and populations. To be useful to fisheries management, the model would have to be adapted to the specific location and goals of the fishery under study. Fishery selectivity of certain size classes or harvest locations could be factored into the model through mortality rates or population/length distribution. Already, models exist that consider the pressures of fishing on shellfish populations [21]. Different species and fishing areas have different regulations. These parameters could be fine-tuned to specific species and fisheries, generating an accurate

representation of the impact of ocean acidification on already-pressured shellfish populations.

Finally, the structure of this model and the program itself should be reviewed for use in environmental assessments. The implications of ocean acidification are not limited to sea scallops, nor to the Atlantic coast. This phenomenon impacts ecosystems across the world. The structure and function of this study's model could be easily applied to a wide range of environmental conditions. Such application would increase the world's understanding of the impact that a changing climate and acidifying oceans have on our marine ecosystems.

7 Acknowledgments

The author of this study thanks Dr. Patrick Haley for his assistance with equations and project code, Dr. Pierre Lermusiaux for his support in constructing well-defined project goals, Ms. Michelle Park and Mr. Alan Zhu for their proofreading, and Joy Xu for her support in streamlining project procedure. Additionally, the author of this study is grateful for the sponsorship of Dr. Fang Zhu and Ms. Qian Zou, Mr. and Mrs. Gerald Mackaman, Dr. Mark Hughes and Dr. Delia Sang, and Zachary Frankel, Ph.D. Finally, the author thanks the Center for Excellence in Education, the Research Science Institute, and the Massachusetts Institute of Technology for the opportunity to assemble this research paper.

References

[1] D. J. Hofmann, J. H. Butler, and P. P. Tans. A new look at atmospheric carbon dioxide. *Atmospheric Environment*, 43(12):2084–2086, 2009.

[2] P. Friedlingstein, M. W. Jones, M. O'Sullivan, R. M. Andrew, D. C. Bakker, J. Hauck, C. Le Quéré, G. P. Peters, W. Peters, J. Pongratz, et al. Global carbon budget 2021. *Earth System Science Data*, 14(4):1917–2005, 2022.

[3] G. J. MacDonald. Scientific basis for the greenhouse effect. *Journal of Policy Analysis and Management*, 7(3):425–444, 1988.

[4] N. Konduru, P. Lindner, and N. M. Assaf-Anid. Curbing the greenhouse effect by carbon dioxide adsorption with zeolite 13X. *AIChE journal*, 53(12):3137–3143, 2007.

[5] D. Toebelmann and T. Wendler. The impact of environmental innovation on carbon dioxide emissions. *Journal of Cleaner Production*, 244:118787, 2020.

[6] Y. Artioli, J. C. Blackford, M. Butenschön, J. T. Holt, S. L. Wakelin, H. Thomas, A. V. Borges, and J. I. Allen. The carbonate system in the North Sea: sensitivity and model validation. *Journal of Marine Systems*, 102:1–13, 2012.

[7] C. A. Hartin, B. Bond-Lamberty, P. Patel, and A. Mundra. Ocean acidification over the next three centuries using a simple global climate carbon-cycle model: projections and sensitivities. *Biogeosciences*, 13(15):4329–4342, 2016.

[8] D. K. Gledhill, M. M. White, J. Salisbury, H. Thomas, I. Mlsna, M. Liebman, B. Mook, J. Grear, A. C. Candelmo, R. C. Chambers, et al. Ocean and coastal acidification off New England and Nova Scotia. *Oceanography*, 28(2):182–197, 2015.

[9] Z. A. Wang, R. Wanninkhof, W.-J. Cai, R. H. Byrne, X. Hu, T.-H. Peng, and W.-J. Huang. The marine inorganic carbon system along the Gulf of Mexico and Atlantic coasts of the United States: Insights from a transregional coastal carbon study. *Limnology and Oceanography*, 58(1):325–342, 2013.

[10] K. E. Harris, M. D. DeGrandpre, and B. Hales. Aragonite saturation state dynamics in a coastal upwelling zone. *Geophysical Research Letters*, 40(11):2720–2725, 2013.

[11] A. W. Miller, A. C. Reynolds, C. Sobrino, and G. F. Riedel. Shellfish face uncertain future in high CO2 world: influence of acidification on oyster larvae calcification and growth in estuaries. *Plos one*, 4(5):e5661, 2009.

[12] J. Salisbury, M. Green, C. Hunt, and J. Campbell. Coastal acidification by rivers: a threat to shellfish? *Eos, Transactions American Geophysical Union*, 89(50):513–513, 2008.

[13] R. D. Brumbaugh, M. W. Beck, L. D. Coen, L. Craig, and P. Hicks. A practitioners guide to the design & monitoring of shellfish restoration projects: an ecosystem services approach. 2006.

[14] C. G. Jones, J. H. Lawton, and M. Shachak. Organisms as ecosystem engineers. In *Ecosystem management*, pages 130–147. Springer, 1994.

[15] D. Narita, K. Rehdanz, and R. S. Tol. Economic costs of ocean acidification: a look into the impacts on global shellfish production. *Climatic Change*, 113(3):1049–1063, 2012.

[16] Commercial landings. *U.S. National Marine Fisheries Service*, 2019.

[17] R. C. Tian, C. Chen, K. D. Stokesbury, B. J. Rothschild, G. W. Cowles, Q. Xu, S. Hu, B. P. Harris, and M. C. Marino II. Modeling the connectivity between sea scallop populations in the Middle Atlantic Bight and over Georges Bank. *Marine Ecology Progress Series*, 380:147–160, 2009.

[18] A. Lisi, C. Hodgdon, and C. Ober. Sea scallop assessment on Stellwagen Bank 2021. 2021.

[19] Z. Zang, R. Ji, D. R. Hart, C. Chen, L. Zhao, and C. S. Davis. Modeling Atlantic sea scallop (Placopecten magellanicus) scope for growth on the Northeast US Shelf. *Fisheries Oceanography*, 31(3):271–290, 2022.

[20] A. Hawkins, P. Duarte, J. Fang, P. Pascoe, J. Zhang, X. Zhang, and M. Zhu. A functional model of responsive suspension-feeding and growth in bivalve shellfish, configured and validated for the scallop Chlamys farreri during culture in China. *Journal of Experimental Marine Biology and Ecology*, 281(1-2):13–40, 2002.

[21] S. R. Cooley, J. E. Rheuban, D. R. Hart, V. Luu, D. M. Glover, J. A. Hare, and S. C. Doney. An integrated assessment model for helping the United States sea scallop (Placopecten magellanicus) fishery plan ahead for ocean acidification and warming. *PLoS One*, 10(5):e0124145, 2015.

[22] M. Alunno-Bruscia, Y. Bourlès, D. Maurer, S. Robert, J. Mazurié, A. Gangnery, P. Goulletquer, and S. Pouvreau. A single bio-energetics growth and reproduction model for the oyster Crassostrea gigas in six Atlantic ecosystems. *Journal of sea research*, 66(4):340–348, 2011.

[23] Application of a population dynamics model to the Mediterranean mussel, Mytilus galloprovincialis, reared in Thau Lagoon (France), author=Gangnery, Aline and Bacher, Cédric and Buestel, Dominique, journal=Aquaculture, volume=229, number=1-4, pages=289–313, year=2004, publisher=Elsevier.

[24] S. A. L. M. Kooijman and S. A. L. M. Kooijman. *Dynamic energy and mass budgets in biological systems*. Cambridge university press, 2000.

[25] T. Troost, J. Wijsman, S. Saraiva, and V. Freitas. Modelling shellfish growth with dynamic energy budget models: an application for cockles and mussels in the Oosterschelde (southwest Netherlands). *Philosophical Transactions of the Royal Society B: Biological Sciences*, 365(1557):3567–3577, 2010.

[26] Dynamic energy budget theory restores coherence in biology, author=Sousa, Tânia and Domingos, Tiago and Poggiale, J-C and Kooijman, SALM. *Philosophical Transactions of the Royal Society B: Biological Sciences*, 365(1557):3413–3428, 2010.

[27] Y. Zhao, J. Zhang, F. Lin, J. S. Ren, K. Sun, Y. Liu, W. Wu, and W. Wang. An ecosystem model for estimating shellfish production carrying capacity in bottom culture systems. *Ecological Modelling*, 393:1–11, 2019.

[28] D. R. Hart. Individual-based yield-per-recruit analysis, with an application to the Atlantic sea scallop, Placopecten magellanicus. *Canadian Journal of Fisheries and Aquatic Sciences*, 58(12):2351–2358, 2001.

[29] M. D. of Marine Fisheries. Commercial shellfish & sea urchin regulations, 2021.

[30] S. Andersen, E. S. Grefsrud, and T. Harboe. Effect of increased pCO 2 level on early shell development in great scallop (Pecten maximus Lamarck) larvae. *Biogeosciences*, 10(10):6161–6184, 2013.

[31] O. Heilmayer, T. Brey, and H.-O. Pörtner. Growth efficiency and temperature in scallops: a comparative analysis of species adapted to different temperatures. *Functional Ecology*, pages 641–647, 2004.

[32] D. R. Hennen and D. R. Hart. Shell height-to-weight relationships for Atlantic sea scallops (Placopecten magellanicus) in offshore US waters. *Journal of Shellfish Research*, 31(4):1133–1144, 2012.

[33] E. R. Lewis and D. W. R. Wallace. Program developed for CO_2 system calculations. Technical Report CDIAC-105, Oak Ridge National Laboratory, Oak Ridge, Tennessee, 1998.

[34] I. Hansson. A new set of acidity constants for carbonic acid and boric acid in sea water. In *Deep Sea Research and Oceanographic Abstracts*, volume 20, pages 461–478. Elsevier, 1973.

[35] A. Dickson and F. J. Millero. A comparison of the equilibrium constants for the dissociation of carbonic acid in seawater media. *Deep Sea Research Part A. Oceanographic Research Papers*, 34(10):1733–1743, 1987.

[36] A. G. Dickson. Standard potential of the reaction: AgCl (s)+ 12H2 (g)= Ag (s)+ HCl (aq), and and the standard acidity constant of the ion HSO4- in synthetic sea water from 273.15 to 318.15 K. *The Journal of Chemical Thermodynamics*, 22(2):113–127, 1990.

[37] J. P. Wheeler. 50th Northeast regional stock assessment workshop (SAW) stock assessment review committee (SARC) meeting monkfish (Lophius americanus) sea scallop (Placopecten magellanicus). 2010.

[38] D. R. Hart. Quantifying the tradeoff between precaution and yield in fishery reference points. *ICES Journal of Marine Science*, 70(3):591–603, 2013.

[39] P. Haley, A. Gupta, C. Mirabito, and P. F. Lermusiaux. Towards Bayesian ocean physical-biogeochemical-acidification prediction and learning systems for Massachusetts Bay. In *Global Oceans 2020: Singapore–US Gulf Coast*, pages 1–9. IEEE, 2020.

[40] J. Salisbury, D. Vandemark, C. Hunt, J. Campbell, B. Jonsson, A. Mahadevan, W. McGillis, and H. Xue. Episodic riverine influence on surface DIC in the coastal Gulf of Maine. *Estuarine, Coastal and Shelf Science*, 82(1):108–118, 2009.

[41] C. Gilbert, W. Gentleman, C. Johnson, C. DiBacco, J. Pringle, and C. Chen. Modelling dispersal of sea scallop (Placopecten magellanicus) larvae on Georges Bank: The influence of depth-distribution, planktonic duration and spawning seasonality. *Progress in Oceanography*, 87(1-4):37–48, 2010.

[42] J. G. Stanley and M. A. Sellers. Species profiles: life histories and environmental requirements of coastal fishes and invertebrates (mid-atlantic): American oyster. 1986.

[43] M. Saunders. A study of the enhancement of american oyster (crassostrea virginica) in southern prince edward island. 2019.

[44] B. J. Rothschild, J. S. Ault, P. Goulletquer, and M. Héral. Decline of the chesapeake bay oyster population: a century of habitat destruction and overfishing. *Marine Ecology Progress Series*, pages 29–39, 1994.

[45] J. M. Harding, R. Mann, and M. J. Southworth. Shell length-at-age relationships in james river, virginia, oysters (crassostrea virginica) collected four centuries apart. *Journal of Shellfish Research*, 27(5):1109–1115, 2008.

[46] M. J. Wilberg, M. E. Livings, J. S. Barkman, B. T. Morris, and J. M. Robinson. Overfishing, disease, habitat loss, and potential extirpation of oysters in upper chesapeake bay. *Marine Ecology Progress Series*, 436:131–144, 2011.

[47] K. Augusto, G. Holmes, and N. Barnes. Massachusetts shellfish aquaculture economic impact study. *Cape Cod Cooperative Extension, Woods Hole Sea Grant and Southeastern Massachusetts Aquaculture Center*, 2015.

A Appendix

A.1 Shellfish Growth Model Pseudocode

Shellfish:

- Get_input_parameters
- Set_initial_conditions
- Loop_over_all_time
  - Read_data
  - Update_shellfish
  - Save_shellfish
- Close files

Get_input_parameters:

- Fetch initial parameters for growth model

Set_initial_conditions:

- Open MIT-MSEAS PE, output files for shellfish
- Input initial conditions (e.g., population distribution of shellfish, boundary parameters)

Read_data:

- Read salinity from MIT-MSEAS PE
- Read total alkalinity from MIT-MSEAS PE
- Read dissolved inorganic carbon from MIT-MSEAS PE

- Read temperature from MIT-MSEAS PE

Update_shellfish:

- Compute_G
- Compute_R
- Get M
- Total count of scallops in each size class calculated here

Save_shellfish:

- Save output

Compute_G:

- Get H_∞
- Compute_H
- Compute_$K_{T,\Omega}$
- Growth matrix calculated here

Compute_R:

- Get α_R
- Get γ_R
- Compute_$scaled_SSB$
- Total recruitment calculated here

Compute_$K_{T,\Omega}$

- Compute_$K_{i_}$ + _Δ_K_t
- Compute_Δ_K_Ω
- Total change in K due to temperature and aragonite calculated here

Compute_$scaled_SSB$

- Compute_$scale_factor$
- Scaled SSB calculated here

Compute_$K_{i_}$ + _Δ_K_t

- Get M_∞
- Get temperature from MIT-MSEAS PE
- Initial K plus change in K due to temperature calculated here

Compute_Δ_K_Ω

- Compute_ΔG
- Get K_i
- Change in K due to change in aragonite calculated here

Compute_$scale_factor$

- Get average survival
- Get aragonite scale factor coefficient
- Get survival intercept
- Get aragonite from MIT-MSEAS PE
- Scale factor applied to spawning stock biomass calculated here

Compute_Δ_G

- Get delta growth aragonite coefficient
- Get delta growth intercept
- Compute_$\Delta\Omega$
- Relative change in growth calculated here

Compute_$\Delta\Omega$

- Get aragonite from MIT-MSEAS PE
- Get $\Omega_{control}$
- Relative change in aragonite from the control value calculated here